

# Depth imaging in anisotropic media by symmetric non-stationary phase shift

Robert J. Ferguson<sup>1\*</sup> and Gary F. Margrave<sup>2</sup>

<sup>1</sup>*Department of Geological Sciences, Campus Mail code C1100, University of Texas, Austin, TX 78712, USA, and* <sup>2</sup>*Consortium for Research in Elastic Wave Exploration Seismology (CREWES), University of Calgary, Canada*

Received March 2000, revision accepted October 2001

## ABSTRACT

We present a new depth-imaging method for seismic data in heterogeneous anisotropic media. This recursive explicit method uses a non-stationary extrapolation operator to allow lateral velocity variation, and it uses the relationship between phase angle and the spectral coordinates of seismic data to allow velocity variation with phase angle. A qualitative comparison of migration impulse responses suggests that, for an equivalent cost, the symmetric non-stationary phase-shift (SNPS) operator is superior to the phase-shift plus interpolation (PSPI) operator, for very large depth intervals. To demonstrate the potential of the new method, seismic data from a physical model acquired over a transversely isotropic medium are imaged using a shot-record migration based on the SNPS operator.

## INTRODUCTION

In seismic imaging, much effort is spent on estimating the elastic parameters (P- and S-wave velocities) of an assumed isotropic subsurface for the construction of seismic images. Thomsen (1986) pointed out the inconsistency of these efforts when the subsurface is potentially anisotropic. Martin, Ehinger and Rasolofosaon (1992) demonstrated that isotropic algorithms applied to physical modelling data in transversely isotropic (TI) media produce mispositioning of plane reflectors and steep structures. Isaac and Lawton (1999) showed that a TI medium having a symmetry axis of 45° (measured from the vertical) causes large errors in the lateral position of a simulated reef edge – errors large enough for an exploratory well to be significantly mispositioned.

Various authors have presented depth-imaging methods for TI media. They include Meadows, Coen and Liu (1987), who extended the imaging method of Stolt (1978) to homogeneous media with elliptical anisotropy; Uren, Gardner and McDonald (1990), who presented a 2D post-stack Stolt method for homogeneous TI; Gonzalez, Lynn and Robinson

(1991), who used an approximate anelliptic dispersion relationship to implement a prestack Stolt method for P-waves in a homogeneous TI medium; Sena and Toksöz (1993), who presented a 2D Kirchhoff algorithm (prestack) for weak TI (Thomsen 1986); Uzcategui (1995), who used explicit depth extrapolators for TI media having a vertical axis of symmetry; Meadows and Abriel (1994), who presented a 3D post-stack phase-shift time algorithm for a homogeneous TI medium to improve the image of data from the Gulf of Mexico; Kitchenside (1993), who proposed a 2D algorithm for homogeneous TI media that constructs an extrapolator in the Fourier domain ( $k_x-\omega$ ) and applies it as a truncated and tapered filter in the space–frequency ( $x-\omega$ ) domain; and Le Rousseau (1997) and Ferguson and Margrave (1998), who presented depth-imaging methods for heterogeneous TI media that are restricted to coincident source–receiver acquisition geometry. Le Rousseau’s (1997) method is based on the phase-shift plus interpolation (PSPI) operator of Gazdag and Sguazzero (1984), and Ferguson and Margrave’s (1998) method is based on the non-stationary phase-shift (NSPS) operator of Margrave and Ferguson (1999).

Most of the above depth-imaging approaches restrict the TI in the medium. Meadows and Abriel (1994), Kitchenside

---

\*E-mail: fergusonr@mail.utexas.edu. Formerly at <sup>2</sup>.

(1993) and Gonzalez *et al.* (1991) assumed homogeneous TI. Meadows *et al.* (1987) assumed elliptical TI. Sena and Toksöz (1993) assumed weak TI and Uzcategui (1995) assumed TI with a vertical axis of symmetry. Le Rousseau (1997) and Ferguson and Margrave (1998) did not restrict TI in the medium, but restricted the acquisition geometry of the seismic data to coincident source and receiver. No such restrictions are required for the depth-imaging method presented here.

Kitchenside's (1993) method is followed in the initial development of our TI algorithm, but rather than applying a truncated filter in the  $(x-\omega)$  domain, the complete filter is applied in the  $(k_x-\omega)$  domain, and a polynomial fit is used to relate  $(k_x, \omega)$  to the phase angle. The resulting homogeneous phase shift allows variation of velocity in the Fourier coordinates  $(k_x, \omega)$  and with depth  $z$ . Generalization to heterogeneous TI is then achieved using the symmetric non-stationary phase-shift (SNPS) operator of Margrave and Ferguson (1999).

A qualitative comparison of PSPI, NSPS and SNPS operators for TI media is presented to illustrate their relative accuracy. A wavefield consisting of a null background in which a number of impulses are embedded is extrapolated a large distance through a strongly varying, TI velocity field that has a non-zero axis of symmetry. The resulting impulse responses are then reversed through the same field. The TI SNPS operator is found to recover the input more accurately through this inversion process at no additional cost.

Physical model data acquired over a dipping TI medium are successfully imaged using a shot-record migration that is based on the SNPS operator. Comparison with migrations based on PSPI or NSPS are omitted as the depth intervals involved are small (less than 10 m) and differences are subtle. A large-depth-step comparison of these operators for use in velocity analysis and datuming is planned for a future paper.

## STATIONARY PHASE SHIFT FOR TI MEDIA

Depth imaging in a homogeneous TI medium (anisotropy is stationary in the lateral coordinates) is simple to develop from the stationary phase-shift method of Gazdag (1978). In this method, the spectrum of the recorded seismic wavefield is recursively extrapolated downwards. At each depth level, as the wavefield moves down, an imaging condition is invoked to form the output data. Generalization of this method from isotropic to anisotropic media uses the relationship between horizontal slowness and wavenumber  $k_x$  with temporal frequency  $\omega$ .

The phase-shift extrapolator central to the Gazdag (1978) method is

$$\psi(x, z, \omega) = \frac{1}{2\pi} \int \alpha(k_x, z, \omega) \varphi(k_x, 0, \omega) \exp(-ixk_x) dk_x, \quad (1)$$

where the monochromatic (in temporal frequency  $\omega$ ) wavefield  $\psi(z)$  is deduced from the  $k_x$  spectrum of  $\varphi(z=0)$ . Equation (1) converts the spectrum  $\varphi$  to space coordinates as a product with  $\alpha$ . In 2D,  $\alpha$  is given by

$$\alpha(k_x, z, \omega) = \exp\left(iz\sqrt{\left(\frac{\omega}{v}\right)^2 - k_x^2}\right), \quad (2)$$

where extrapolation is in the positive  $z$ -direction and  $v$  is the velocity in the medium. The velocity  $v$  in (2) is kept constant in all lateral coordinates and phase angles, and variation of  $v$  with depth is achieved by recursive extrapolation. Thus, the medium to be imaged must be homogeneous in the lateral coordinate and also isotropic.

Similarly to the method of Kitchenside (1993), the relationship between horizontal slowness  $p$  and  $(k_x, \omega)$  and phase angle  $\theta$ ,

$$p = \frac{\sin(\theta)}{v(\theta)} = \frac{k_x}{\omega}, \quad (3)$$

is used with the P-wave velocity  $v(\theta)$  computed using (Thomsen 1986)

$$v(\theta)^2 = \alpha_0^2 [1 + \varepsilon \sin^2(\theta) + D^*(\theta)], \quad (4)$$

where

$$D^*(\theta) = \frac{1}{2} \left[ 1 - \beta_0^2 / \alpha_0^2 \right] \left[ -1 + \sqrt{1 + \frac{4\delta^*}{(1 - \beta_0^2 / \alpha_0^2)^2} \sin^2(\theta) \cos^2(\theta)} + \sqrt{\frac{4\varepsilon(1 - \beta_0^2 / \alpha_0^2 + \varepsilon)}{(1 - \beta_0^2 / \alpha_0^2)^2} \sin^4(\theta)} \right]. \quad (5)$$

The parameters  $\alpha_0$ ,  $\beta_0$ ,  $\varepsilon$  and  $\delta^*$  in (4) and (5) are the following functions of the four elastic constants  $C_{11}$ ,  $C_{33}$ ,  $C_{44}$  and  $C_{13}$  (Thomsen 1986):

$$\alpha_0 = \sqrt{\frac{C_{33}}{\rho}}, \quad \beta_0 = \sqrt{\frac{C_{44}}{\rho}}, \quad (6)$$

and

$$\varepsilon = \frac{C_{11} - C_{33}}{2C_{33}},$$

$$\delta^* = \frac{1}{2C_{33}^2} \left[ 2(C_{13} + C_{44})^2 - (C_{33} - C_{44})(C_{11} + C_{33} - 2C_{44}) \right]. \quad (7)$$

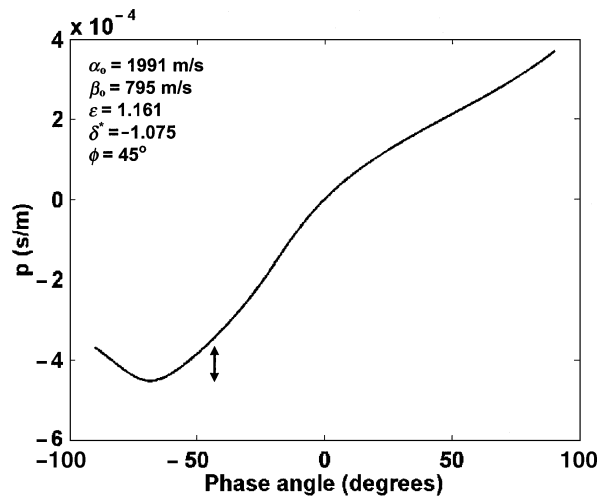


Figure 1 Plot of slowness  $p = k_x/\omega$  versus phase angle  $\theta$  for a dipping TI medium (the anisotropic parameters and dip are inset). Each value of  $p$  in the range indicated by the arrow corresponds to two phase angles. Values outside of this range are uniquely defined.

If the TI medium is dipping (i.e. the axis of TI symmetry is not vertical), (3) must be rotated by the angle between the axis of TI symmetry and the vertical. In Fig. 1, the horizontal slowness  $p$  for weathered gypsum (anisotropic parameters from Thomsen 1986) is plotted against phase angle  $\theta$ . A polynomial fit to this curve provides an empirical relationship between  $\theta$  and  $p$ :

$$\theta(k_x, \omega) = a_0 + a_1 \frac{k_x}{\omega} + a_2 \left(\frac{k_x}{\omega}\right)^2 + \dots + a_n \left(\frac{k_x}{\omega}\right)^n, \quad (8)$$

where  $a_i$  are the polynomial coefficients. (The appropriate value of  $n$  is determined by numerical experimentation.) At every  $(k_x, \omega)$  in  $\varphi(0)$ , a phase angle  $\theta$  is defined for (3) using the polynomial (8) and the associated velocity is computed using (4). The phase-shift symbol (equation (2)) becomes

$$\alpha(k_x, z, \omega) = \exp\left(iz\sqrt{\left(\frac{\omega}{v(\theta(k_x, \omega))}\right)^2 - k_x^2}\right), \quad (9)$$

where  $v$  is now no longer constant but is a functional of  $\theta$ .

We prefer to use the polynomial relationship between  $(k_x, \omega)$  and  $\theta$  because of the cumbersome nature of their analytic relationship (roots of quartic equations must be found). Also, in even the most strongly TI media,  $p$  versus  $\theta$  curves can be easily fitted with fewer than 20 coefficients in the non-evanescent region. The overhead associated with the polynomials, when compared with a similarly configured isotropic

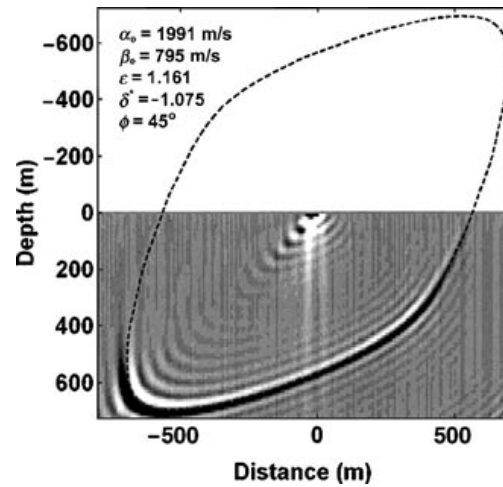


Figure 2 The impulse response for phase shift in a homogeneous TI medium with an axis of symmetry of  $45^\circ$ . The dashed curve shows the theoretical response. The impulse response does not track the theoretical response beyond  $90^\circ$  (left side of figure).

operator, increases the runtime by a factor of five when coefficients are computed and stored prior to the runtime.

A difficulty presents itself when the axis of symmetry  $\phi$  of a TI medium is non-zero (Tsvankin 1997). In Fig. 1, a plot of horizontal slowness,  $p = k_x/\omega$ , versus phase angle  $\theta$  for a dipping TI medium shows that some values of  $p$  correspond to two values of  $\theta$ . The result of ambiguity in  $\theta$  for this range of  $p$  can be seen in the depth-migration impulse response shown in Fig. 2. The response is unable to track the theoretical curve (the solid line) beyond  $90^\circ$  (the left side of the image) as it lies in the evanescent region of the spectrum. The turning wave migration of Hale, Hill and Stefani (1992) is suggested as a remedy.

### SYMMETRIC NON-STATIONARY PHASE SHIFT FOR TI MEDIA

Symmetric non-stationary phase shift (SNPS) (Margrave and Ferguson 1999) uses non-stationary filter theory (Margrave 1998) to allow velocity variation in the lateral coordinate. The resulting symmetric operator is more accurate and more stable than other explicit wavefield extrapolators (Margrave and Ferguson 1999). In 2D, the SNPS extrapolator is written,

$$\psi(x, z, \omega) = \int \psi(y, 0, \omega) \frac{1}{2\pi} \int \alpha\left(x, k_x, \frac{z}{2}, \omega\right) \alpha\left(y, k_x, \frac{z}{2}, \omega\right) \exp(-ik_x[x - y]) dk_x dy, \quad (10)$$

where, in isotropic media, the product  $\alpha(x)\alpha(y)$  is

$$\alpha\left(x, k_x, \frac{z}{2}, \omega\right)\alpha\left(y, k_x, \frac{z}{2}, \omega\right) = \exp\left(\frac{iz}{2}\sqrt{\left(\frac{\omega}{v(x)}\right)^2 - k_x^2} + \frac{iz}{2}\sqrt{\left(\frac{\omega}{v(y)}\right)^2 - k_x^2}\right). \quad (11)$$

Lateral coordinates at  $z = 0$  (input) are represented by  $y$  and output coordinates at  $z$  (output) are represented by  $x$ . The equivalent linear operator in (10) is symmetric in the coordinates  $x$  and  $y$  (Margrave and Ferguson 1999). In a heterogeneous anisotropic medium, the product  $\alpha(x)\alpha(y)$  (equation (11)) is given by

$$\alpha\left(x, k_x, \frac{z}{2}, \omega\right)\alpha\left(x, k_x, \frac{z}{2}, \omega\right) = \exp\left(\frac{iz}{2}\sqrt{\left(\frac{\omega}{v(x, \theta(k_x, \omega))}\right)^2 - k_x^2} + \frac{iz}{2}\sqrt{\left(\frac{\omega}{v(y, \theta(k_x, \omega))}\right)^2 - k_x^2}\right), \quad (12)$$

where  $v$  as a function of  $\theta$  is given in (8).

An efficient implementation of (10) for isotropic media is obtained by splitting the extrapolation into two steps (Ferguson and Margrave 1999). Each step proceeds as a set of stationary phase shifts corresponding to a P-wave velocity profile that is piecewise continuous laterally. The extension to TI simply requires replacement of each  $\alpha$  in (11) with its anisotropic description (equation (9)).

**Accuracy**

A qualitative comparison of anisotropic PSPI, NSPS and SNPS is presented to indicate the improved accuracy of SNPS. The PSPI operator used here is implemented as a non-stationary combination filter (Margrave 1998) with no interpolation step. For each operator, a wavefield consisting of two impulses embedded in a null background (Fig. 3) is extrapolated a large distance (500 m) through the strongly heterogeneous anisotropic medium of Fig. 4. The resulting wavefields (Figs 5a, 6a and 7a) are reversed the same distance using the corresponding operators (Figs 5b, 6b and 7b). In this forward-and-back sequence, the invertible operator recovers band-limited impulses similar to Fig. 3.

Because SNPS is a cascade of NSPS and PSPI, extrapolation through 500 m is split into two extrapolations each of 250 m, thus approximately doubling the computational cost of SNPS compared with PSPI and NSPS. For a fair

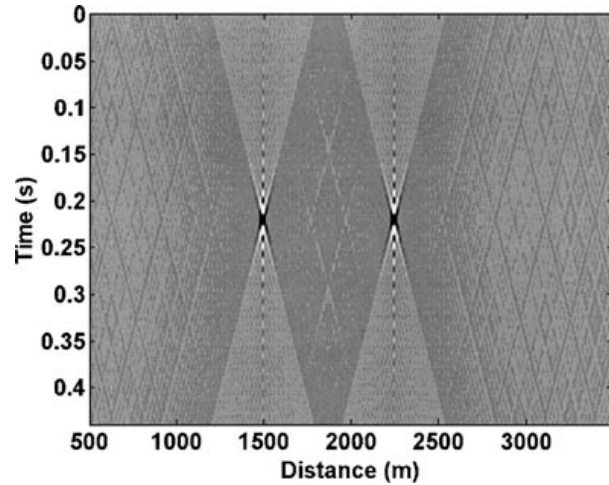


Figure 3 Impulses in a null background.

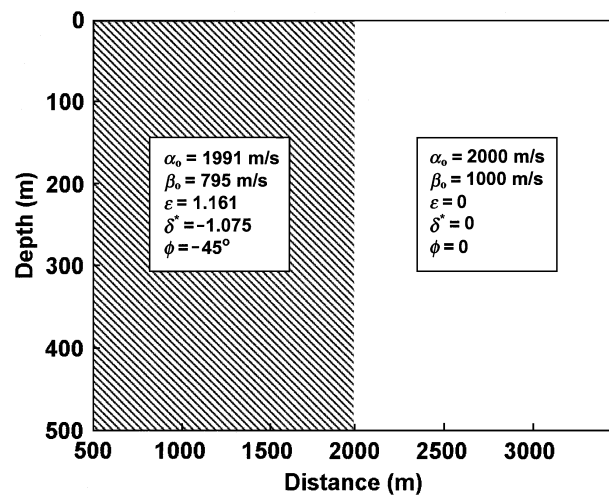


Figure 4 A heterogeneous anisotropic medium. The shaded region represents a dipping TI medium (the anisotropic parameters are inset). The solid region is isotropic.

comparison, the PSPI and NSPS results in Figs 6 and 7 are computed in two steps of 250 m, so the same extrapolation distance is covered for a computational cost that is equivalent to SNPS.

As can be seen in Fig. 7(b), SNPS provides a better image of the impulses than PSPI (Fig. 5b) or NSPS (Fig. 6b). Two spurious hyperbolae lie between the impulses in Fig. 5(b) (PSPI) and in Fig. 6(b) (NSPS). Similar hyperbolae are present in Fig. 7(b) (SNPS) but at much lower amplitude. (Figs 5b, 6b and 7b are scaled to maximum amplitude.) No formal proof is given here to establish the equivalence of invertibility and

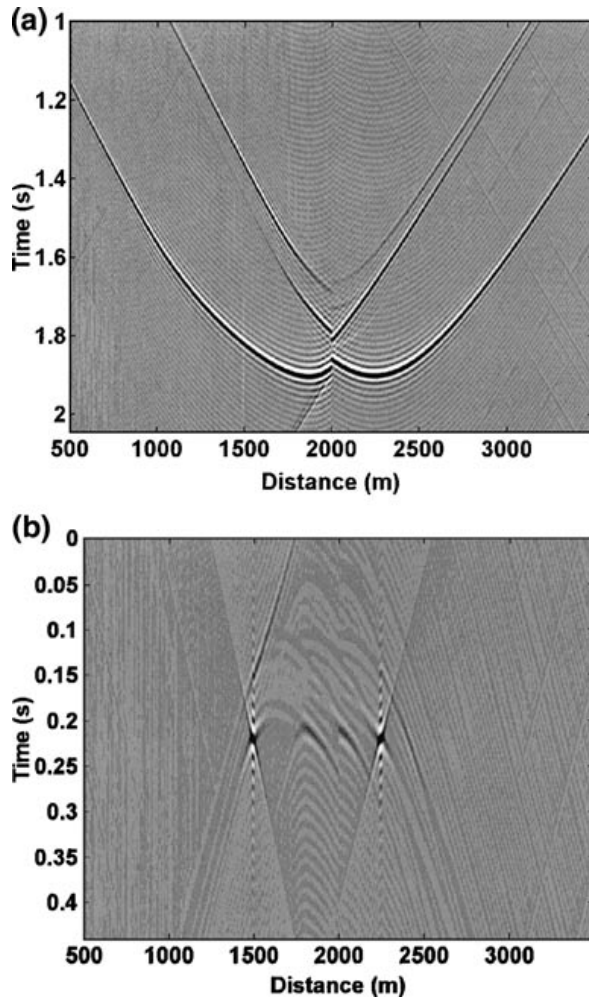


Figure 5 PSPI: Forward and reverse propagation of the impulses in Fig. 3 through the medium in Fig. 4: (a) forward; (b) reverse.

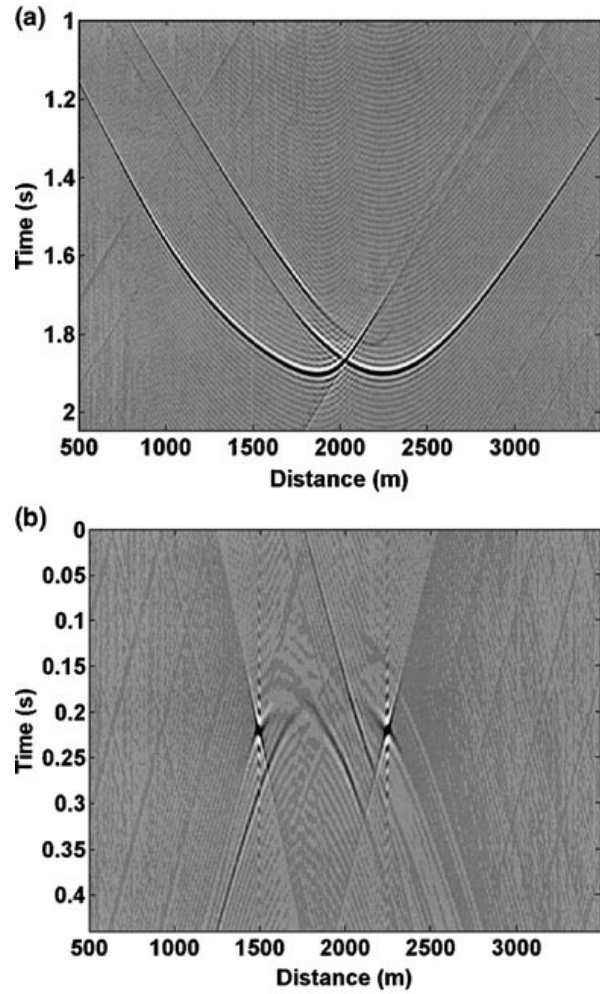


Figure 6 NSPS: Forward and reverse propagation of the impulses in Fig. 3 through the medium in Fig. 4: (a) forward; (b) reverse.

accuracy; however, the perfect invertibility (in the non-evanescent region) of stationary phase shift suggests that invertibility and accuracy are closely related.

**ANISOTROPIC THRUST SHEET EMBEDDED IN AN ISOTROPIC BACKGROUND**

A shot-record migration based on the SNPS operator is used to image a heterogeneous TI medium. The migration follows closely the isotropic migration of Ferguson and Margrave (2002), where shots and receivers are propagated separately, and it uses the TI SNPS operator developed above. A gridded depth model is required, with TI parameters plus the angle-of-symmetry axis specified for each gridpoint.

The data were acquired at the Physical Modeling Facility, University of Calgary by the Foothills Research Project (now the Fold-Fault Research Project). The physical model consists of a TI thrust sheet embedded in an isotropic background (Fig. 8). The sheet is composed of four blocks of phynolic material (a mixture of canvas and resin), and each block has a different axis of TI symmetry. The scale of the model is 1000:1, and the Thomsen (1986) parameters are  $\alpha_0 = 2870$  m/s,  $\beta_0 = 1570$  m/s,  $\epsilon = 0.223$  and  $\delta^* = 0.204$ . The isotropic background is Plexiglas with a P-wave velocity of 2740 m/s. The base of the model is a flat aluminium plate. Sonic transducers were used as sources and receivers with a source spacing of 60 m and receiver spacing of 20 m. The recording geometry varies along the line from 91 traces

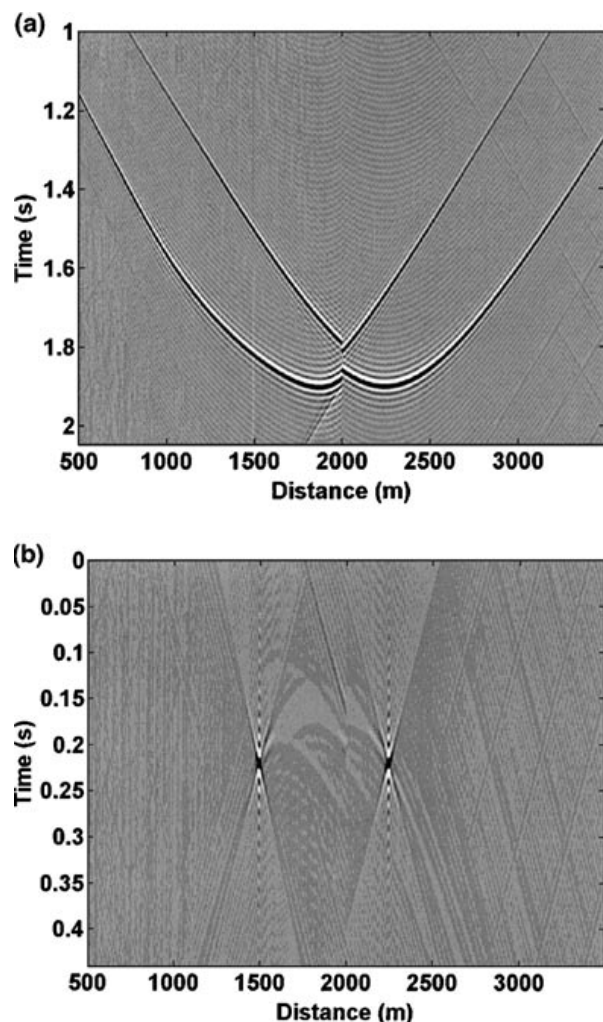


Figure 7 SNPS: Forward and reverse propagation of the impulses in Fig. 3 through the medium in Fig. 4: (a) forward; (b) reverse.

single-sided at the start of the line, to 182 traces split-spread in the middle, to 91 traces single-sided at the end of the line. Absolute near- and far-offsets are 200 m and 2000 m, respectively, and 86 shot-records were acquired.

A shot gather is shown in Fig. 9 and spans the first 4000 m of the model. The shotpoint is at 2040 m. The major reflection at the bottom of the gather is from the aluminium plate. To the left of the source location, energy has propagated mainly through the isotropic Plexiglas, the phynolic with a symmetry axis of 30°, and the block of VTI (vertical axis of TI symmetry) material. The corresponding reflection has a continuous appearance, suggesting simple raypaths. To the right of the source, reflected energy has propagated through the TI blocks with the steeper axes of TI symmetry. The resulting apparent moveout on the reflection is discontinuous, suggesting more complicated raypaths than on the left side. Reflections from joints between the TI blocks are apparent on the near-offsets between 0.3 s and 0.8 s two-way time.

Figure 10 shows the depth migration of the source gather in Fig. 9 using a shot-record migration based on the TI-SNPS operator. The aluminium plate is imaged at the correct depth on both sides of the source (compare with Fig. 8). The lack of continuity directly below the source location is due to the 200 m gap in the near-offsets on the source gather (Fig. 9). Images of the two shallowest joints between the TI blocks are visible at depths 450 m and 950 m, although, because of the limited recording aperture of a single shot, they are poorly imaged.

All 86 shot-records were imaged singly, and then stacked to form a single image (Fig. 11). The images of the two shallowest joints are significantly improved as a result of the constructive interference of images from multiple shots. Continuity of the base reflector is very good, with some amplitude loss between 2200 m and 2400 m laterally.

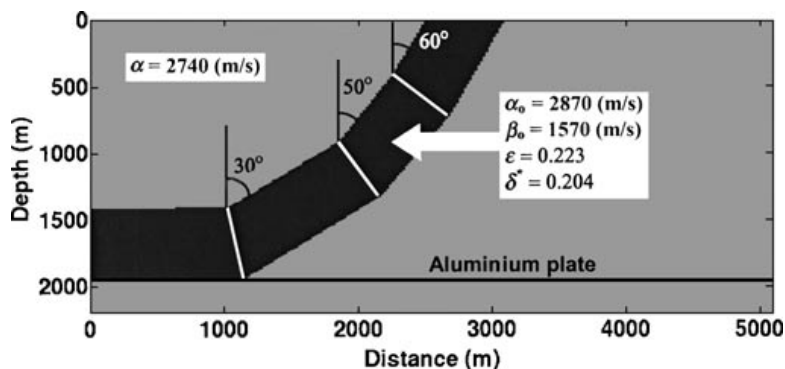


Figure 8 Model of a TI thrust sheet embedded in an isotropic background. The thrust sheet is composed of four blocks of TI material with the same anisotropic parameters (inset). Each block has a unique axis of TI symmetry.

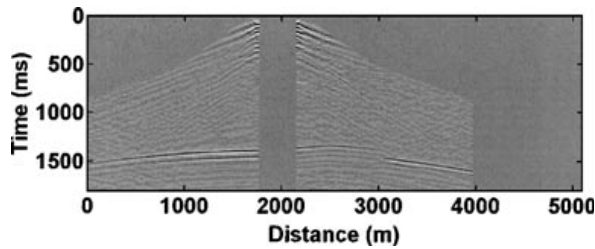


Figure 9 Shot gather corresponding to source location 2040 m in Fig. 8. The major reflection at the bottom of the section corresponds to the base of the model. The apparent moveout of the reflection to the left of the source is continuous because most of the reflection energy propagated only through the isotropic material part of the model and the TI block with the vertical axis of symmetry. The reflection energy to the right of the source has propagated through the three blocks with non-vertical axes of TI symmetry and so appears discontinuous.

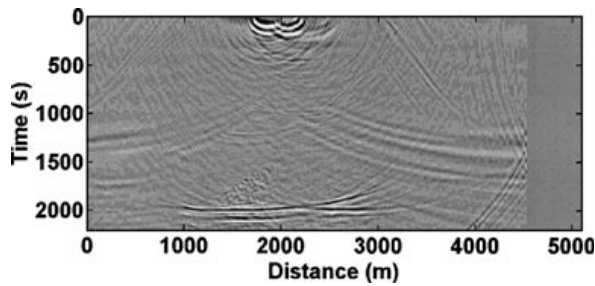


Figure 10 TI depth image corresponding to the shot gather in Fig. 9. The base of the model is correctly imaged. The discontinuity of the image below the shot location corresponds to the gap between the live traces (Fig. 9).

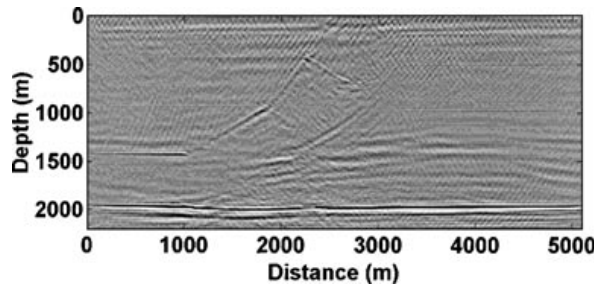


Figure 11 Stack of TI shot-migrated gathers. The base of the model and the joints between the TI blocks are correctly imaged.

A common-image-point (CIP) gather, corresponding to 2300 m (Fig. 12), shows that only three or four shot gathers between 3000 m and 3300 m contribute significant energy to the image of the base reflection, while those between 1750 m

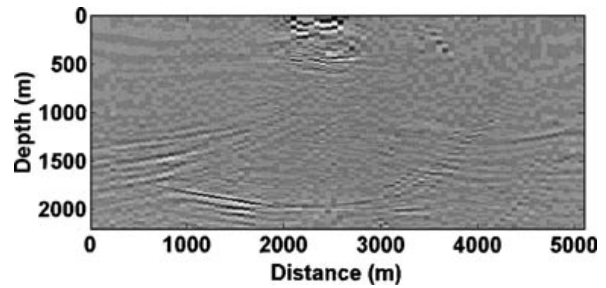


Figure 12 Common-image-point (CIP) gather corresponding to the distance of 2300 m on Fig. 11. Only those shots between 3000 m and 3300 m contribute significant wave energy to the image of the base reflector. Shots between 1750 m and 3000 m, located above the steepest part of the thrust sheet, contribute less energy. The steep part of the thrust may act as a local waveguide, deflecting energy away from the base reflector between 2200 m and 2400 m.

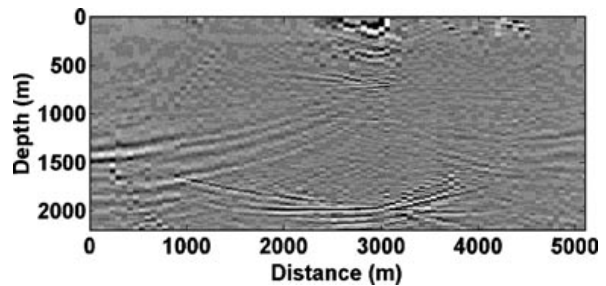


Figure 13 CIP corresponding to the distance of 2800 m on Fig. 11. Shots between 1750 m and 3300 m contribute most of the wave energy to the image of the base reflector. Here, the energy is less affected by the waveguide effect than the CIP of Fig. 12.

and 3000 m contribute energy of relatively low amplitude. For the latter range, the steep part of the thrust may be acting as a local waveguide, deflecting down-going waves away from the base reflector, and/or, after reflection, deflecting waves away from the recording aperture. In contrast, in Fig. 13, a nearby CIP gather (2800 m) shows consistent amplitude from the same range of shots (1750 m to 3300 m).

## CONCLUSIONS

A new depth-imaging method for dipping TI media was presented based on the symmetric non-stationary phase-shift (SNPS) operator. It was adapted for depth imaging in a TI medium by relating the coordinates of the seismic spectrum to phase angle through a polynomial fit. The choice of the SNPS operator in preference to PSPI or NSPS operators was justified by comparing forward and reverse propagation of impulses

through a thick, heterogeneous TI medium. Of the three operators, the SNPS operator recovered the input impulses with the least distortion. Data from a TI physical model were successfully depth-imaged using a shot-record migration, based on the anisotropic SNPS operator. The steeply dipping parts of the model possibly acted as waveguides, causing localized dimming of reflection energy from a flat event.

## REFERENCES

- Ferguson R.J. and Margrave G.F. 1998. Depth migration in TI media by non-stationary phase shift. 68th SEG meeting, New Orleans, USA, Expanded Abstracts, 1831–1834.
- Ferguson R.J. and Margrave G.F. 1999. A practical implementation of symmetric non-stationary phase shift. 69th SEG meeting, Houston, USA, Expanded Abstracts, SPRO 11.5.
- Ferguson R.J. and Margrave G.F. 2002. Prestack depth migration by symmetric non-stationary phase shift. *Geophysics*, in press.
- Gazdag J. 1978. Wave equation migration with the phase shift method. *Geophysics* **43**, 1342–1351.
- Gazdag J. and Sguazzero P. 1984. Migration of seismic data by phase shift plus interpolation. *Geophysics* **49**, 124–131.
- Gonzalez A., Lynn W. and Robinson W.F. 1991. Prestack frequency-wavenumber (f-k) migration in transversely isotropic medium. 61st SEG meeting, Houston, USA, Expanded Abstracts, 1155–1157.
- Hale D., Hill N.R. and Stefani J. 1992. Imaging salt with turning waves. *Geophysics* **57**, 1453–1463.
- Isaac J.H. and Lawton D.C. 1999. Image mispositioning due to dipping TI media: a physical seismic modeling study. *Geophysics* **64**, 1230–1238.
- Kitchenside P.W. 1993. 2D anisotropic migration in the space-frequency domain. *Journal of Seismic Exploration* **2**, 7–22.
- Le Rousseau J.H. 1997. Depth migration in heterogeneous, transversely isotropic media with the phase-shift-plus-interpolation method. 67th SEG meeting, Dallas, USA, Expanded Abstracts, 1703–1706.
- Margrave G.F. 1998. Theory of non-stationary linear filtering in the Fourier domain with application to time-variant filtering. *Geophysics* **63**, 244–259.
- Margrave G.F. and Ferguson R.J. 1999. An explicit symmetric wavefield extrapolator for depth migration. 69th SEG meeting, Houston, USA, Expanded Abstracts, SPRO 14.4.
- Martin D., Ehinger A. and Rasolofosaon P.N.J. 1992. Some aspects of seismic modeling and imaging in anisotropic media using laser ultrasonics. 62nd SEG meeting, New Orleans, USA, Expanded Abstracts, 1373–1376.
- Meadows M.A. and Abriel W.L. 1994. 3D phase-shift migration in transversely isotropic media. 64th SEG meeting, Los Angeles, USA, Expanded Abstracts, 1331–1348.
- Meadows M.A., Coen S. and Liu G. 1987. F-K migration in elliptically anisotropic media. 57th SEG meeting, New Orleans, USA, Expanded Abstracts, 659–661.
- Sena A.G. and Toksöz M.N. 1993. Kirchhoff migration and velocity analysis for converted and nonconverted waves in anisotropic media. *Geophysics* **58**, 265–276.
- Stolt R. 1978. Migration by Fourier transform. *Geophysics* **43**, 23–48.
- Thomsen L. 1986. Weak elastic anisotropy. *Geophysics* **51**, 1954–1966.
- Tsvankin I. 1997. Moveout analysis for transversely isotropic media with a tilted symmetry axis. *Geophysical Prospecting* **45**, 479–512.
- Uren N.F., Gardner G.H.F. and McDonald J.A. 1990. The migrator's equation for anisotropic media. *Geophysics* **55**, 1429–1434.
- Uzcategui O. 1995. 2D depth migration in transversely isotropic media using explicit operators. *Geophysics* **60**, 1819–1829.